Control on the density and optical properties of color centers at SiO_2/SiC interfaces by oxidation and annealing

Takato Nakanuma,[1,a)] Kosuke Tahara,[2] Katsuhiro Kutsuki,[2] Takayoshi Shimura,[1] Heiji Watanabe,[1] and Takuma Kobayashi[1,a)]

[1] *Graduate School of Engineering, Osaka University, Suita, Osaka 565-0871, Japan*

[2] *Toyota Central R&D Labs., Inc., Nagakute, Aichi 480-1192, Japan*

[a)] Authors to whom correspondence should be addressed:

nakanuma@ade.prec.eng.osaka-u.ac.jp and kobayashi@prec.eng.osaka-u.ac.jp

Color centers in solids can serve as single photon emitters (SPEs) that are important in many quantum applications. Silicon carbide (SiC) is a promising host for color centers because of its well-established crystal growth and device technologies. Although color centers with extremely high brightness were found at the silicon dioxide (SiO_2)/SiC interface, controlling their density and optical properties remains a challenge. In this study, we demonstrate control over the color centers at the SiO_2/SiC interface by designing the oxidation and annealing conditions. We report that post-oxidation CO_2 annealing has the ability to reduce the color centers at the interface and form well-isolated SPEs with bright emission. We also discuss the correlation between the color centers and electrically active defects.

Solid-state single photon emitters (SPEs) find various applications in quantum computing[1], quantum cryptography[2], and quantum sensing[3]. Optically active point defects (i.e., color centers) in wide bandgap semiconductors can serve as SPEs. Furthermore, if the color center possesses a non-zero spin ground state, it may act as a spin-to-photon interface[2,4]. The nitrogen-vacancy center (N*V* center) in diamond is a leading example; the spin state of N*V* centers can be optically initialized, manipulated, and detected even at room temperature[5–7]. Group-IV color centers such as silicon-vacancy (Si*V*)[8] and germanium-vacancy (Ge*V*)[9] centers in diamond are also attractive because of their extremely high Debye-Waller factor and sharp zero phonon transition.

Silicon carbide (SiC) is a wide gap semiconductor that shares favorable properties for quantum technology with diamond[10,11]. Wafer-scale crystal growth, well-controlled *n*- and *p*-type doping, and mature device technologies make this material attractive as a host for SPEs[12,13]. A number of color centers have been found in bulk SiC so far, e.g. silicon-vacancy (V_{Si})[14,15], divacancy ($V_{Si}V_C$)[16,17], carbon antisite-vacancy complex ($C_{Si}V_C$)[18], and nitrogen-vacancy center (N_CV_{Si})[19–21]. Among them, coherent control of defect spins for V_{Si}[15], $V_{Si}V_C$[17], and N_CV_{Si}[21] have been demonstrated at room temperature. While these defects are important candidates for qubits, color centers with extremely bright emission have also been found at the SiO_2/SiC interface[22–26]. These centers exhibit single photon emission within the visible spectrum at room temperature, with a count rate exceeding that of the NV center in diamond[23,24]. Moreover, they can be readily implemented in semiconductor devices, enabling control of their luminescence by electrical current or voltage[23,24]. However, achieving control over their density and optical properties is not straightforward. A previous study suggested that stable color centers start to form during the oxidation of SiC at 550°C, but their density remains almost constant within a wide oxidation temperature range of 700–1100°C[22]. It was also noted that the color center density is oxide thickness dependent[25], but the magnitude of the change is rather small. This may impede the formation of spatially well-separated SPEs at the SiO_2/SiC interface. Additionally, achieving controllability over the optical properties is challenging. Unstable color centers are frequently found at the interface unless the process conditions are carefully designed[22,25]. It is also known that the emission spectrum from the defects strongly varies among them, even within the very same sample chip[23–25]. Understanding the microscopic origin of defects is crucial for better control over them. Although carbon defects[27–31] and/or oxygen defects (i.e., defect complexes in SiC[32,33] and oxygen vacancies in SiO_2[34,35]) in SiO_2/SiC structures are possible candidates, the details are still unclear. Investigating the correlation between optically and electrically active defects should provide a hint regarding the origin of defects. Such attempts have been made in this regard[25,26], but

further investigation involving samples processed under various conditions is needed to deepen the understanding.

In this study, we aim to control the density and optical properties of color centers at the SiO_2/SiC interface by designing the oxide formation conditions. In particular, we investigate the impact of high-temperature oxidation[36] and post-oxidation annealing in a carbon dioxide (CO_2) ambient[37]. Both methods are known to effectively reduce the electrical defects in SiC metal-oxide-semiconductor (MOS) devices. Although post-oxidation annealing in nitric oxide (NO) ambient is the most common method to improve the SiO_2/SiC interface quality, it is known that the NO annealing leads to the formation of very fast interface states due to the incorporation of a high amount of nitrogen atoms[38]. We use the high-temperature oxidation and CO_2 annealing to avoid introducing any foreign atoms into the SiO_2/SiC system. This enables us to focus on the intrinsic defects in the SiO_2/SiC structure (excluding possible defects involving nitrogen donors), which simplifies the situation. It should be noted that the oxide growth during the CO_2 annealing can be ignored, because the activation energy of oxidation by CO_2 is much high (7.5 eV) compared with that by O_2 (2.9 eV)[37]. Therefore, the CO_2 annealing is likely effective in reducing the interface carbon defects and oxide defects while preventing the oxide growth. We also discuss the correlation between the density of color centers and electrically active defects to gain insights into the origin of color centers.

The flow of sample preparation and measurements is shown in Fig. 1. *N*-type 4H-SiC(0001) substrates with 5 μm-thick epilayers (donor density: 1.0×10^{16} cm^{-3}) are used in this study. After wet cleaning and the removal of surface oxide by 10%-diluted hydrofluoric (HF) acid, we form the SiO_2/SiC structures through two different processes: (i) thermal oxidation at 1200–1500°C in 100% O_2 ambient and (ii) thermal oxidation at 1200°C followed by annealing in CO_2 at 1050–1200°C for 30 min. Note that the samples were cooled down without gas replacement. Hereafter, these samples are labeled by conditions, e.g., Ox. 1200°C and Ox.+CO_2 1050°C. The resulting oxide thickness ranges from 18–34 nm. Optical measurements are performed on SiO_2/SiC samples, and electrical measurements are conducted on SiC MOS capacitors with Al gate electrodes. All measurements are conducted at room temperature.

We describe the details of optical measurements. Figure 1(b) shows the schematic of our homemade confocal microscope. An excitation laser with a wavelength of $\lambda = 532$ nm is focused onto the SiO_2/SiC interface using an objective lens with NA=0.9 (MPLAPON60X, Olympus). The resulting photoluminescence (PL) is collected by the same objective lens, passed through a dichroic mirror (550 nm cut-on), and detected either by the spectrometer (HRS-300 and Pixis100BRX,

Teledyne Princeton Instruments) or by the avalanche photodiode-based single photon counting modules (SPCM-AQRH-14, Excelitas Technologies). The objective lens is placed on top of the piezoelectric stage, which enables a three-dimensional mapping of the PL intensity. A 600-nm long-pass filter is inserted after the dichroic mirror to cutoff the Raman lines when taking the PL mapping image. Hanbury-Brown and Twiss (HBT) measurement[39,40] is also performed to evaluate the single photon property of the defects. For this measurement, the photons are passed through the 600-nm long-pass filter, split by the 50:50 beam splitter, and detected by either of the two single photon counting modules. Then, the difference in the timing of single photon detection by the two modules is analyzed with the multiscaler (MCS8A, FAST Comtec).

Figure 2 shows typical PL mapping images of SiO_2/SiC samples. A large number of color centers is observed in the Ox. 1200°C sample (Fig. 2(a)), which is comparatively low in the Ox. 1500°C sample (Fig. 2(b)). Hence, it seems that high-temperature oxidation is effective in reducing the color center density. For quantitative discussion, we evaluate the density of color centers with count rates greater than 5.0×10^4 counts/sec through image processing. As a result, color center densities are 5.2×10^7, 2.0×10^7, 1.6×10^7, and 1.2×10^7 cm^{-2} for samples oxidized at 1200, 1300, 1400, and 1500°C, respectively. Thus, the density decreases monotonically as the oxidation temperature increases. However, the density stays in the same order of magnitude (10^7 cm^{-2}) even when the temperature is increased up to 1500°C. As explained in the following paragraph, reducing the density of color centers is crucial to make them act as SPEs. We then take a look into the PL mapping image for the CO_2-annealed samples (Figs. 2(c) and 2(d)). We see that the color center density is substantially lower in the annealed samples compared with the as-oxidized ones (Figs. 2(a) and 2(b)). In particular, when the CO_2 anneal is performed at a high temperature of 1200°C, only three spots with a count rate higher than 5.0×10^4 counts/sec are observed in the 30×30 μm^2 area (Fig. 2(d)). Again, image processing is performed to quantitatively investigate the color center density as a function of CO_2 anneal temperature. The resulting color center densities are 2.9×10^6, 1.4×10^6, 5.6×10^5, and 3.3×10^5 cm^{-2} for samples annealed at 1050, 1100, 1150, and 1200°C, respectively. Compared with the Ox. 1200°C sample, the color center density becomes two orders of magnitude smaller after CO_2 annealing at 1200°C. Thus, CO_2 annealing has the ability to reduce not only the electrically active defects[37] but also the color centers at the SiO_2/SiC interface.

Figures 3(a) and 3(b) show the typical PL spectra of the Ox. 1200°C and Ox.+CO_2 1200°C samples measured at room temperature. Find all the measured spectra for these samples in the supplementary information. Note that the two sharp peaks located above 2.2 eV, regardless of the

sample conditions, are the transverse and longitudinal optic Raman signals of 4H-SiC crystal[23,41,42]. The luminescence of color centers appears as broad signals in the energy range of 1.5 – 2.2 eV. For the as-oxidized sample (Fig. 3(a)), the shape, intensity, and peak position of PL spectra strongly vary among the investigated defects, in agreement with previous reports[23,24]. In contrast, the color centers in the CO_2-annealed sample (Fig. 3(b)) more frequently exhibit similar PL signals, as represented by the defects #2–#4. This suggests that CO_2 annealing is effective in reducing the variation in the optical signals. This reduction could be due to a decrease in the types of color centers and/or to the reduction in the charge/strain in the local environment around the defect. Then, the single photon properties of the defects are evaluated through HBT measurements, where typical results are shown in Figs. 3(c) and 3(d). Note that the second-order correlation function, $g^{(2)}(\tau)$ is calculated without background subtraction in this study. While anti-bunching behavior is observed for the investigated defects, the $g^{(2)}(0)$ values do not reach below 0.5 for several of the defects (e.g., #4) in the Ox. 1200°C sample (Fig. 3(c)). This means that the color centers in the as-oxidized sample are not isolated SPEs. In fact, we find that only 12 out of the investigated 18 diffraction limited confocal spots exhibited SPE characteristics for the Ox. 1200°C sample. The high density of color centers (Fig. 2(a)) may contribute to the background signal superimposed on the defect signal of interest, thereby degrading the SPE characteristics. In contrast, the $g^{(2)}(0)$ values are well below 0.5 for the Ox.+CO_2 1200°C sample (Fig. 3(d)). We confirm that 11 out of the investigated 11 defects in the Ox.+CO_2 1200°C sample behave as SPEs. While the CO_2 anneal leaves defects with relatively low PL intensities (Fig. 3(c)), the count rates are still very high ($> 5.5\times10^4$ counts/sec) after annealing at 1200°C. Therefore, CO_2 annealing is effective not only in reducing the number of color centers but also in forming well-isolated and bright SPEs at the SiO_2/SiC interface.

Finally, we discuss the relationship between the optically and electrically active defects. Figure 4 shows typical capacitance–voltage (C–V) characteristics for the Ox. 1200°C and Ox.+CO_2 1200°C samples measured at 1 MHz. The gate voltage is swept forward (depletion to accumulation) and then backward (accumulation to depletion). The Ox. 1200°C sample exhibits a large positive flatband voltage (V_{FB}) shift as well as a significant C–V hysteresis. These positive V_{FB} shift and C–V hysteresis likely correspond to the effective fixed charge (mostly related to deep acceptor-type interface states) and the near-interface oxide traps, respectively. The plausible candidates for the interface states and near-interface oxide traps are carbon-related defects[27–31] and oxygen vacancies[34,35], respectively. In the Ox.+CO_2 1200°C sample, both the V_{FB} shift and the hysteresis are clearly suppressed. Hence, CO_2 annealing is effective in passivating the interface defects and near-interface oxide traps, in accordance

with a previous study[37]. In this study, two types of electrical traps were estimated from the *C–V* characteristics, i.e., deep interface traps and near-interface oxide traps. The former is evaluated from the V_{FB} shift, while the latter is evaluated from the *C–V* hysteresis. Here, we reasonably assume that the positive V_{FB} shift observed in SiC MOS structures is mainly caused by interface traps with deep trap levels. The areal density of charges corresponding to the V_{FB} shift ($N_{eff.}$) and *C–V* hysteresis ($N_{hys.}$) for each sample condition is shown together with the color center density in Fig. 5. We find that the color center density is more closely related to $N_{eff.}$ than $N_{hys.}$ This indicates that the color centers correlate with the deep interface defects rather than the near-interface oxide traps. This does not contradict with the previous study which stated that the color centers are located at the SiC-side of the interface[22]. On the other hand, it is notable that the density of color centers is five orders of magnitude smaller than that of electrically active defects. This means that only a part of the electrically active defects is detected as color centers. As mentioned earlier, a possible cause for the observed color centers is the oxidation induced defects consist of carbon and/or oxygen atoms. They likely induce deep trap levels at the SiO_2/SiC interface which could be reduced either by high-temperature oxidation or CO_2 annealing.

In summary, we investigated the impact of oxidation and annealing treatment on the density and optical properties of color centers at the SiO_2/SiC interface. Although the color center density remains in the same order (10^7 cm^{-2}) even when changing the oxidation temperature of SiC within the range of 1200°C and 1500°C, we observe a reduction in density by two orders of magnitude through post-oxidation CO_2 annealing at 1200°C. We find that one-third of the investigated color centers in the as-oxidized sample at 1200°C indicate $g^2(0)$ values higher than 0.5 and do not exhibit SPE characteristics. In contrast, all 11 investigated defects behave as SPEs in the sample annealed in CO_2 at 1200°C. Therefore, CO_2 annealing not only reduces the density of color centers but also forms well-isolated SPEs at the SiO_2/SiC interface. Furthermore, we emphasize that the color center is more closely associated with the effective fixed charge rather than the near-interface oxide traps, suggesting that the origin of color centers lies in interface defects with deep trap levels.

Supplementary Material

All of the measured PL spectra of Ox. 1200°C and Ox.+CO_2 1200°C samples can be found in the supplementary information.

Acknowledgments

This work was partly supported by JST, PRESTO Grant Number JPMJPR22B5.

AUTHOR DECLARATIONS

Conflict of Interest

The authors have no conflicts to disclose.

DATA AVAILABILITY

The data that support the findings of this study are available from the corresponding authors upon reasonable request.

REFERENCES

[1] J.R. Weber, W.F. Koehl, J.B. Varley, A. Janotti, B.B. Buckley, C.G. Van De Walle, and D.D. Awschalom, Proc. Natl. Acad. Sci. U. S. A. **107**, 8513 (2010).

[2] M. Atatüre, D. Englund, N. Vamivakas, S.Y. Lee, and J. Wrachtrup, Nat. Rev. Mater. **3**, 38 (2018).

[3] C.L. Degen, F. Reinhard, and P. Cappellaro, Rev. Mod. Phys. **89**, 1 (2017).

[4] D.D. Awschalom, R. Hanson, J. Wrachtrup, and B.B. Zhou, Nat. Photonics **12**, 516 (2018).

[5] A. Gruber, A. Dräbenstedt, C. Tietz, L. Fleury, J. Wrachtrup, and C. Von Borczyskowski, Science (80-.). **276**, 2012 (1997).

[6] F. Jelezko, T. Gaebel, I. Popa, A. Gruber, and J. Wrachtrup, Phys. Rev. Lett. **92**, 076401 (2004).

[7] F. Jelezko and J. Wrachtrup, Phys. Status Solidi Appl. Mater. Sci. **203**, 3207 (2006).

[8] D.D. Sukachev, A. Sipahigil, C.T. Nguyen, M.K. Bhaskar, R.E. Evans, F. Jelezko, and M.D. Lukin, Phys. Rev. Lett. **119**, 223602 (2017).

[9] M.K. Bhaskar, D.D. Sukachev, A. Sipahigil, R.E. Evans, M.J. Burek, C.T. Nguyen, L.J. Rogers, P. Siyushev, M.H. Metsch, H. Park, F. Jelezko, M. Lončar, and M.D. Lukin, Phys. Rev. Lett. **118**, 223603 (2017).

[10] N.T. Son, C.P. Anderson, A. Bourassa, K.C. Miao, C. Babin, M. Widmann, M. Niethammer, J. Ul Hassan, N. Morioka, I.G. Ivanov, F. Kaiser, J. Wrachtrup, and D.D. Awschalom, Appl. Phys. Lett. **116**, 190501 (2020).

[11] S. Castelletto and A. Boretti, JPhys Photonics **2**, 022001 (2020).

[12] T. Kimoto and J.A. Cooper, *Fundamentals of Silicon Carbide Technology* (2014).

[13] T. Kimoto and H. Watanabe, Appl. Phys. Express **13**, 120101 (2020).

[14] V. Ivády, J. Davidsson, N.T. Son, T. Ohshima, I.A. Abrikosov, and A. Gali, Phys. Rev. B **96**, 161114 (2017).

[15] M. Widmann, S.Y. Lee, T. Rendler, N.T. Son, H. Fedder, S. Paik, L.P. Yang, N. Zhao, S. Yang, I. Booker, A. Denisenko, M. Jamali, S. Ali Momenzadeh, I. Gerhardt, T. Ohshima, A. Gali, E. Janzén, and J. Wrachtrup, Nat. Mater. **14**, 164 (2015).

[16] D.J. Christle, A.L. Falk, P. Andrich, P. V. Klimov, J.U. Hassan, N.T. Son, E. Janzén, T. Ohshima, and D.D. Awschalom, Nat. Mater. **14**, 160 (2015).

[17] W.F. Koehl, B.B. Buckley, F.J. Heremans, G. Calusine, and D.D. Awschalom, Nature **479**, 84 (2011).

[18] S. Castelletto, B.C. Johnson, V. Ivády, N. Stavrias, T. Umeda, A. Gali, and T. Ohshima, Nat. Mater. **13**, 151 (2014).
[19] H.J. Von Bardeleben, J.L. Cantin, E. Rauls, and U. Gerstmann, Phys. Rev. B - Condens. Matter Mater. Phys. **92**, 064104 (2015).
[20] Z. Mu, S.A. Zargaleh, H.J. Von Bardeleben, J.E. Fröch, M. Nonahal, H. Cai, X. Yang, J. Yang, X. Li, I. Aharonovich, and W. Gao, Nano Lett. **20**, 6142 (2020).
[21] J.F. Wang, F.F. Yan, Q. Li, Z.H. Liu, H. Liu, G.P. Guo, L.P. Guo, X. Zhou, J.M. Cui, J. Wang, Z.Q. Zhou, X.Y. Xu, J.S. Xu, C.F. Li, and G.C. Guo, Phys. Rev. Lett. **124**, 223601 (2020).
[22] A. Lohrmann, S. Castelletto, J.R. Klein, T. Ohshima, M. Bosi, M. Negri, D.W.M. Lau, B.C. Gibson, S. Prawer, J.C. McCallum, and B.C. Johnson, Appl. Phys. Lett. **108**, 021107 (2016).
[23] A. Lohrmann, N. Iwamoto, Z. Bodrog, S. Castelletto, T. Ohshima, T.J. Karle, A. Gali, S. Prawer, J.C. McCallum, and B.C. Johnson, Nat. Commun. **6**, 7783 (2015).
[24] Y. Abe, T. Umeda, M. Okamoto, R. Kosugi, S. Harada, M. Haruyama, W. Kada, O. Hanaizumi, S. Onoda, and T. Ohshima, Appl. Phys. Lett. **112**, 031105 (2018).
[25] Y. Hijikata, S. Komori, S. Otojima, Y.I. Matsushita, and T. Ohshima, Appl. Phys. Lett. **118**, 204005 (2021).
[26] B.C. Johnson, J. Woerle, D. Haasmann, C.T.K. Lew, R.A. Parker, H. Knowles, B. Pingault, M. Atature, A. Gali, S. Dimitrijev, M. Camarda, and J.C. McCallum, Phys. Rev. Appl. **12**, 044024 (2019).
[27] V. V. Afanasev, M. Bassler, G. Pensl, and M. Schulz, Phys. Stat. Sol. **162**, 321 (1997).
[28] P. Deák, J.M. Knaup, T. Hornos, C. Thill, A. Gali, and T. Frauenheim, J. Phys. D. Appl. Phys. **40**, 6242 (2007).
[29] T. Umeda, G.W. Kim, T. Okuda, M. Sometani, T. Kimoto, and S. Harada, Appl. Phys. Lett. **113**, 061605 (2018).
[30] T. Kobayashi and T. Kimoto, Appl. Phys. Lett. **111**, 062101 (2017).
[31] T. Kobayashi and Y.I. Matsushita, J. Appl. Phys. **126**, 145302 (2019).
[32] Y. Hijikata, T. Horii, Y. Furukawa, Y.I. Matsushita, and T. Ohshima, J. Phys. Commun. **2**, 111003 (2018).
[33] Y.-I. Matsushita, Y. Furukawa, Y. Hijikata, and T. Ohshima, Appl. Surf. Sci. **464**, 451 (2019).
[34] J.M. Knaup, P. Deák, T. Frauenheim, A. Gali, Z. Hajnal, and W.J. Choyke, Phys. Rev. B **72**, 115323 (2005).
[35] E. Okuno, T. Sakakibara, S. Onda, M. Itoh, and T. Uda, Phys. Rev. B **79**, 113302 (2009).

[36] T. Hosoi, D. Nagai, M. Sometani, Y. Katsu, H. Takeda, T. Shimura, M. Takei, and H. Watanabe, Appl. Phys. Lett. **109**, 182114 (2016).
[37] T. Hosoi, M. Ohsako, T. Shimura, and H. Watanabe, Appl. Phys. Express **14**, 101001 (2021).
[38] H. Yoshioka, T. Nakamura, and T. Kimoto, J. Appl. Phys. **112**, 024520 (2012).
[39] R. Hanbury Brown and R.Q. Twiss, J. Astrophys. Astron. **177**, 27 (1956).
[40] C. Kurtsiefer, S. Mayer, P. Zarda, and H. Weinfurter, Phys. Rev. Lett. **85**, 290 (2000).
[41] B. Lienhard, T. Schröder, S. Mouradian, F. Dolde, T.T. Tran, I. Aharonovich, and D. Englund, Optica **3**, 768 (2016).
[42] J.C. Burton, L. Sun, F.H. Long, Z.C. Feng, and I.T. Ferguson, Phys. Rev. B **59**, 7282 (1999).

FIGURES

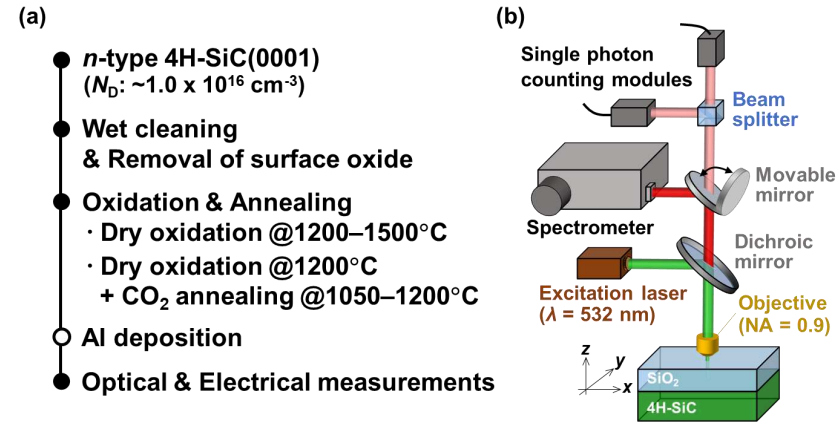

Fig. 1. (a) Flow of sample preparation and measurements and (b) schematic view of our in-house-built confocal microscope setup.

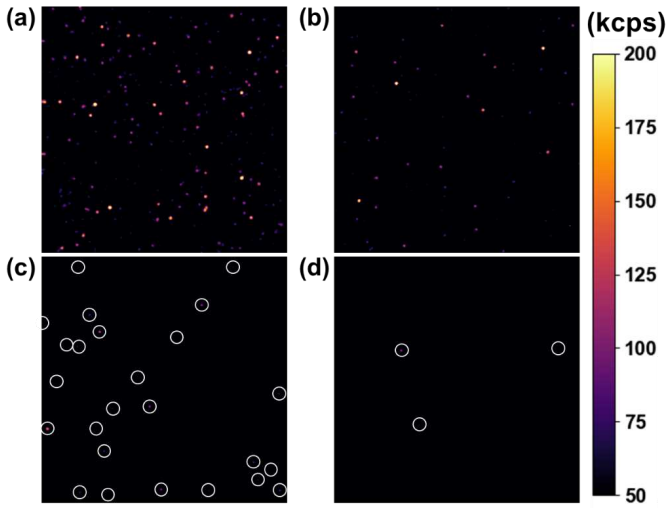

Fig. 2. Confocal PL mapping images of SiO_2/SiC samples (area: 30×30 μm^2): (a) Ox. 1200°C, (b) Ox. 1500°C, (c) Ox.+CO_2 1050°C, and (d) Ox.+CO_2 1200°C. Excitation laser power is set to 0.5 mW. For (c) and (d), the color centers with a count rate higher than 5.0×10^4 counts/sec are circled as guides.

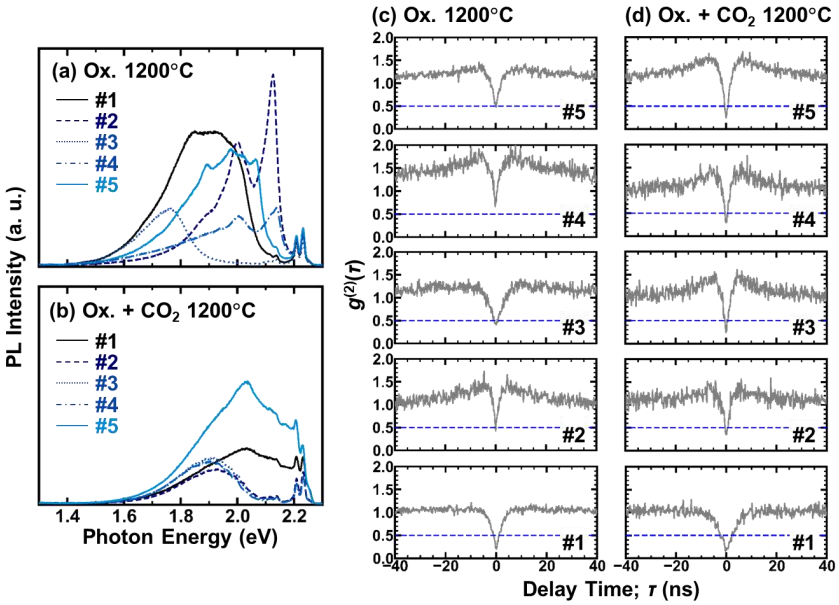

Fig. 3. (a)(b) PL spectra for five different color centers observed in (a) Ox. 1200°C and (b) Ox.+CO_2 1200°C. (c)(d) Results of HBT measurements without background subtraction for the defects in (c) Ox. 1200°C and (d) Ox.+CO_2 1200°C. Blue dashed lines correspond to the $g^{(2)}(\tau)$ value of 0.5. The sample number #1–#5 in (c) and (d) corresponds to the defect with same number in (a) and (b), respectively.

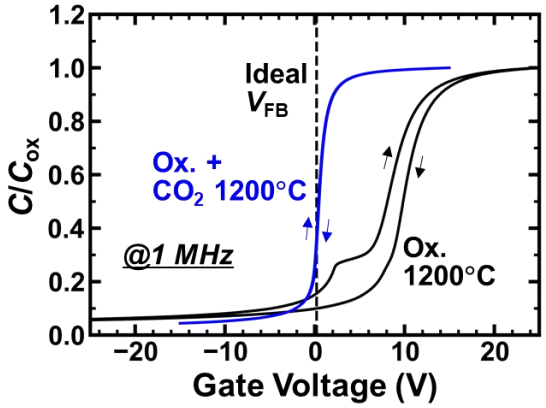

Fig. 4. Bidirectional 1-MHz *C*–*V* characteristics of SiC MOS capacitors: Ox. 1200°C and Ox.+CO_2 1200°C. Dashed line indicates ideal V_{FB} position.

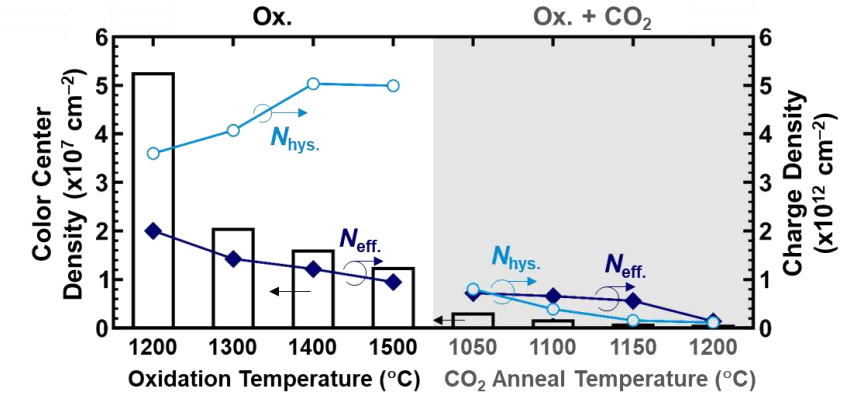

Fig. 5. Density of optically and electrically active defects shown as a function of sample conditions. The density of color centers with a count rate higher than 5.0×10^4 counts/sec is estimated through image processing. The areal density of charges corresponding to the V_{FB} shift ($N_{eff.}$) and C–V hysteresis ($N_{hys.}$) are separately indicated.